PSFC/JA-07-9

Observation of Megagauss Field Topology Changes due to Magnetic Reconnection in Laser- Produced Plasmas

C. K. Li[1], F. H. Séguin[1], R. P. J. Town[2], R. D. Petrasso[1], J. A. Frenje[1], J. P. Knauer[3], O. L. Landen[2], J. R. Rygg[1], V. A. Smalyuk[3]

[1]*Plasma Science and Fusion Center, Massachusetts Institute of Technology, Cambridge, Massachusetts 02139, USA*
[2]*Lawrence Livermore National Laboratory, Livermore, California 94550 USA*
[3]*Laboratory for Laser Energetics, University of Rochester, Rochester, New York 14623, USA*

21 June 2007

Plasma Science and Fusion Center
Massachusetts Institute of Technology
Cambridge, MA 02139 USA

The work described here was performed in part at the LLE National Laser User's Facility (NLUF), and was supported in part by US DOE (Grant No. DE-FG03-03SF22691), LLNL (subcontract Grant No. B504974), and LLE (subcontract Grant No. 412160-001G).

Accepted for publication in ***Physical Review Letters***

Observation of Megagauss Field Topology Changes due to Magnetic Reconnection in Laser-Produced Plasmas

C. K. Li[1], F. H. Séguin[1], R. P. J. Town[2], R. D. Petrasso[1], J. A. Frenje[1], J. P. Knauer[3], O. L. Landen[2], J. R. Rygg[1], V. A. Smalyuk[3]

[1]*Plasma Science and Fusion Center, Massachusetts Institute of Technology, Cambridge, Massachusetts 02139, USA*
[2]*Lawrence Livermore National Laboratory, Livermore, California 94550 USA*
[3]*Laboratory for Laser Energetics, University of Rochester, Rochester, New York 14623, USA*

The spatial structure and temporal evolution of megagauss magnetic fields generated by interactions of up to 4 laser beams with matter were studied with an innovative, time-gated proton radiography method that produces images of unprecedented clarity because it utilizes an isotropic, truly monoenergetic backlighter (14.7-MeV protons from D^3He nuclear fusion reactions). Quantitative field maps reveal precisely and directly, for the first time, changes in the magnetic topology due to reconnection in a high-energy-density plasma ($n_e \sim 10^{20}$–10^{22} cm^{-3}, $T_e \sim 1$ keV).

PACS numbers: 52.38 Fz, 52.50. Jm, 52.70. Nc

The interaction and reconnection of magnetic (B) fields in plasmas are important fundamental processes [1] with direct implications for a wide range of basic sciences, including astrophysics [2], space physics [3] and laboratory physics [4-6]. In the frontier field of high-energy-density (HED) physics (pressures >1 megabar) [7,8], the generation, evolution, and reconnection of B fields due to laser-plasma interactions takes place in an extreme physical regime. High plasma densities (>10^{20} cm^{-3}), high temperatures (~1 keV), intense B fields [~1 megagauss (MG)], and high ratios of thermal pressure to magnetic pressure (β>>1) distinguish this novel regime from tenuous plasmas, of order 10^{14} cm^{-3} or (usually much) lower, that are the more traditional venue of reconnection experiments [1,4]. Here we describe experiments involving the observation of field reconnection in the HED regime, where plasma flow is dominated by hydrodynamics and isn't strongly affected by fields, even though MG fields are present. The results have fundamental implications for basic reconnection physics in all regimes for astrophysics, space physics, and laboratory physics. In addition, the methodology is quite general and is applicable to a wide class of plasma and basic physics experiments. These include, for example, HED physics experiments in which precise, time-resolved field measurements are a necessity [7,8], and experiments involving strongly coupled, Warm Dense Matter (WDM) [9] where the energy loss of monoeneregetic, charged particles can be related to the dynamic interaction between the transiting particles and the WDM [10]

Megagauss B fields are generated in a hot, high-density plasma by illuminating a solid material with a high-power laser beam [11-13]. The laser heats the material, forming an expanding, hemispherical plasma bubble with an intense, toroidal B field on its surface. The dominant source for field generation is non-collinear electron density and temperature gradients ($\nabla n_e \times \nabla T_e$) [11-15]. While the bubble is hot and expanding, the dominant mechanism for field transport is convection [$\nabla\times(\mathbf{v}\times\mathbf{B})$, where $\mathbf{v}$ is the plasma fluid velocity]; at later times, when the laser is off and the cooling plasma becomes more resistive, field diffusion dominates convective transport [ie. $\nabla\times(D_m\nabla\times\mathbf{B})$, where D_m is the magnetic diffusion coefficient].

Recent single-laser-beam experiments [16] at the OMEGA laser facility [17] have demonstrated that the hemispherical bubble radius grows linearly while the laser is on, and then continues to expand after the laser is off. It was shown that the plasma density is in the range $n_e \sim 10^{20}$–10^{22} cm^{-3}, the temperature was $T_e \sim 1$ keV, and the B fields were ~1 MG [11]. It follows that the ratio of the thermal pressure to the field pressure $\beta >> 1$, indicating that plasma motion and field behavior in these bubbles are dominated by plasma fluid dynamics rather than fields [11,16].

When two or more nonoverlapping laser beams are incident on a material, each generates an expanding, conductive plasma bubble with associated magnetic field. If the laser beams are close enough, the bubbles eventually encounter each other with B fields of opposing sign and, presumably, reconnection will occur. The experiments described here were specially designed for mapping the detailed spatial structure and temporal evolution of the fields around multiple bubbles, from the time when lasers were turned on to well after lasers were turned off, allowing the whole processes of field generation and bubble interaction to be observed. In contrast to other important and recently reported two-bubble interaction experiments [13] that postulate reconnection, but for which field maps were not measured, we directly and precisely measure the B field and topological changes due to the reconnection event.

Our experiments were performed at the OMEGA laser facility using laser beams with a wavelength of 0.351 μm in a 1-ns long, square pulse. The energy in each beam was ~500 J, with a spot diameter of 800 μm (containing 95% of beam energy [18]), and the resultant laser intensity was ~ 10^{14} W cm^{-2}. Two or four of these beams (interaction beams) were incident on a 5-μm-thick, plastic (CH) foil.

The novel arrangement used for imaging the spatial structure and temporal evolution of the fields is shown in Fig. 1. The laser-illuminated foil was backlit by protons at the discrete energy of 14.7 MeV produced in fusion reactions ($D+^3He \rightarrow \alpha+p$) in an imploded, D^3He-filled, glass-shell capsule driven by 20 OMEGA laser beams [11,16]. The duration of proton emission from the backlighter was ~150

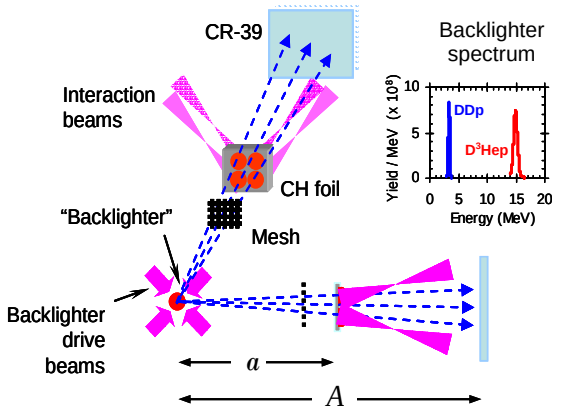

FIG. 1. (Color) Experimental setup. Shown are the proton backlighter (imploded D^3He-filled capsule), mesh, CH foils, CR-39 imaging detectors, and laser beams. The protons forming each image are broken up into beamlets when they pass through a metal mesh (60-μm-thick Ni with 75-μm holes spaced 150 μm center-to-center). Distances from the backlighter were 1.3 cm to mesh, a = 1.5 cm to foil, and A = 30 cm to detector. The measured backlighter spectrum is typical. Yields are ~3×10^8 for D^3He protons and ~4×10^8 for DD protons (separate images can be made with both protons of both energies, but only D^3He-proton images are used here).

ps, and the timing of the interaction laser was adjusted in different experiments so the arrival of the backlighter protons at the foil would occur with different delays after the laser interaction beam was turned on. A metal mesh was placed between the backlighter and the foil to divide the protons into beamlets.

Critical to the implementation of these experiments are the unique properties of the backlighter: it is *pulsed*, truly m*onoenergetic*, and *isotropic*. It is used with imaging detectors (CR-39) that are matched to each type of proton, detect individual protons, and provide information about he energy of each proton [10,19]. Monoenergetic protons provide an unambiguous relationship between the measured lateral deflection of proton beamlets and the strength of any B fields through which they travel. An isotropic backlighter allows images of a large area to be made without variations in proton energy or fluence over the field of view; it also makes possible multiple experiments at different angles around the backlighter, as shown in Fig. 1. The interactions of separate laser-produced bubbles and their B fields are illustrated by the face-on images shown in Figs. 2A and 2B for four and two laser beams, respectively. Figure 2A shows images recorded during 7 shots in which the laser timing was adjusted so the protons arrived at the foil at designated times after the laser interaction beams were turned on. The experiments covered the periods when the beams were on (0.3 to 1 ns) and off (1.2 to 2.4 ns). Figure 2B shows similar data for two laser beams, but at fewer times. The 4-beam and 2-beam experiments differed by having 1.8-mm and 1.4-mm beam spacing (center-to-center), respectively, and by having different angles of incidence on the foil. The beams were incident at 23° from the normal in the 4-beam cases and 47.8° in the 2-beam cases; as a result, the 2-beam illumination was more elliptical (axis ratio ~1.5) and had a correspondingly smaller intensity.

Before interpreting the data it is useful to discuss the structure of an individual laser- generated bubble, which can be visualized with 2-D simulations (current codes are limited to 2-D and cannot simulate multiple beams). Fig. 3 shows simulated spatial distributions of n_e, T_e, and |B| in a plane perpendicular to the foil at times 0.6 ns and1.5 ns (the latter 0.5 ns after the 1-ns laser beam turns off). The laser is assumed incident from the right and the imaging protons are incident from the left, as in Fig. 1. Most important for radiography images are Figs. 3c1 and 3c2, which show that MG magnetic fields are localized on the surface of the bubble (as has recently been experimentally verified [11]). If we imagine protons incident from the left in Fig. 3c1, the direction of the B field is such that the proton trajectories would be deflected slightly in the direction of increasing radius (R). The net effect of these deflections in recorded images is a magnification of the bubble, with larger beamlet spacing inside the bubble than outside. Each bubble seen in the images of Figs. 2A and 2B has an apparent border where

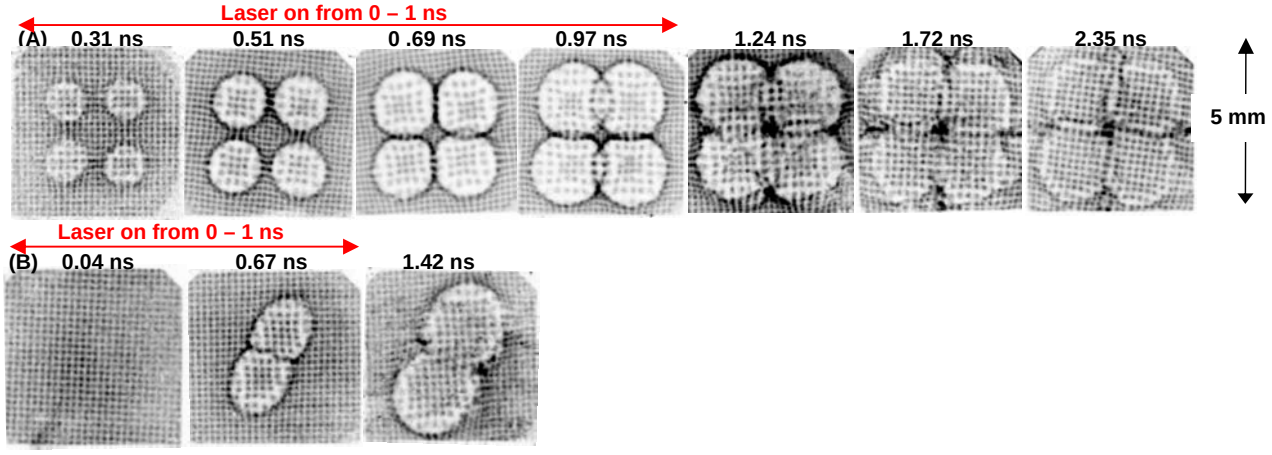

FIG. 2. Radiographs showing the structure and evolution of B fields generated when four (A) or two (B) laser beams are incident on a CH foil. In (A), inter-bubble interactions were minimal while the laser was on (< 1 ns) but significant later. At 1.24 and 1.72 ns asymmetric bubble structure is superposed on a static background pattern that is still visible at 2.35 ns, after most of the bubble structure has dissipated; that pattern is from fields around the burn-through hole (Fig. 3). In (B) there is little distortion at 0.04 ns, but by 0.67 ns the bubbles have interacted and reconnection has occurred. By 1.42 ns most or all of the fields in the intersection region have reconnected, and the distortion remaining in the overlap region is largely due to burn-through holes.

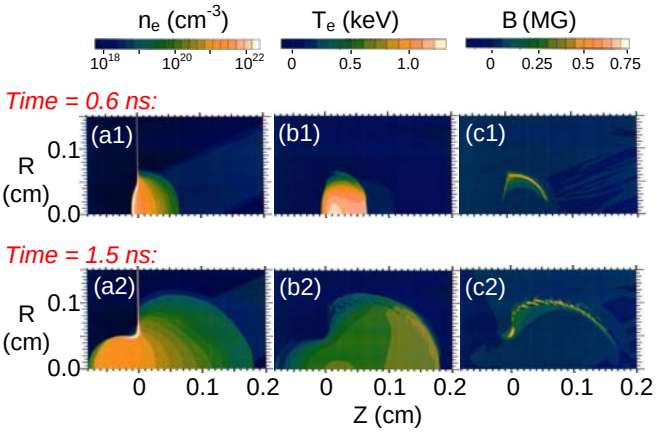

FIG. 3. (Color) Distributions of electron density, electron temperature, and B-field amplitude in an isolated laser-generated plasma bubble, simulated with the 2-D code LASNEX [22]. The parameters used are equivalent to those used in each beam of the 4-beam experiment. The surface of the foil is at position Z = 0.0 on the horizontal axes, and the laser is incident from the right. The field is always perpendicular to the plane of the image. We have shown previously [11,16] that such simulations provide a fairly accurate picture of single-beam interactions while the laser is on, and a qualitative picture that is not quantitatively accurate after the laser is off. In (c1) we see that while the laser is on the B field is localized on the surface of the quasi-hemispherical plasma bubble. In (c2) we see that a strong field structure appears at the edge of the hole burned into the foil some time after the laser is off.

beamlets pile up to for a sharp circular ring, but because of magnification the touching or overlapping of different beamlet-pileup circles in the images from ~ 0.5 to 1 ns do not always indicate that the plasma bubbles and field structures have interacted or even touched yet (see below in Fig. 4).

The displacement $\boldsymbol{\xi}$ of each individual beamlet at the image plane, relative to the position it would have in the image if there were no fields, is

$$\boldsymbol{\xi} = -\frac{qa(A-a)}{A m_p v_p}\int \mathbf{B}\times d\boldsymbol{\ell} \quad , \qquad (1)$$

where q is the electric charge, a and A are the geometric parameters shown in Fig. 1, m_p is the proton mass, v_p is the proton velocity, and $d\boldsymbol{\ell}$ is the differential pathlength along the proton trajectory. This equation can be used to calculate a map of field strength at the foil, using the values of $|\boldsymbol{\xi}|$ for each beamlet.

Sample analyses are shown in Fig. 4 for two of the images from Fig. 2. Figure 4a1 represents a time (0.69 ns) in the 4-beam case before the bubbles grew large enough to touch each other, although the field structure has the effect of magnifying the bubbles and making them appear to overlap in the image. Figure 4b1 shows the measured $\boldsymbol{\xi}$ for each beamlet, and Fig. 4c1 shows the field map (spatial distribution of $|\int \mathbf{B}\times d\boldsymbol{\ell}|$) at the location of the foil. Figure 4d1 shows a lineout through the field map, illustrating the localization of the field on the outside of the bubble; the field structures from the two bubbles don't yet touch each other. The radiograph shown in Fig. 4a2 represents a similar time in the 2-beam experiment. Because of the closer spacing and the elliptical laser footprint described above, the bubbles in this case have collided, as illustrated in Figs. 4b2 and 4c2. The field map (Fig. 4c2) and the lineout (Fig. 4d2) show that the field energy density is substantially smaller in the region of intersection of the two bubbles than in the other regions around the peripheries of the bubbles, indicating that reconnection has occurred. This will be evaluated quantitatively below.

In both 4-beam and the 2-beam sequences, the data show bubble sizes growing while the laser was on with expansion velocity ~5×10^7 cm s^{-1}. Quantitative analysis of the bubble overlap regions is more complicated after the lasers turned off. First, two boundaries appear in the image of each bubble during this time interval. One is the boundary of the bubble, but one is due to B fields that form around the hole burned through the foil by the laser (see Fig. 3c2). At late times, this feature dominates completely (see the last image in Fig. 2A). Second, we've seen previously [16] that the bubbles lose their symmetry after the laser is off (see the second-to-last image of Fig. 2A). Finally, during the period from ~ 1 ns to 2 ns when the image structure is complicated, it is more difficult to identify which beamlet in the image should be identified with which beamlet in the incident proton flux.

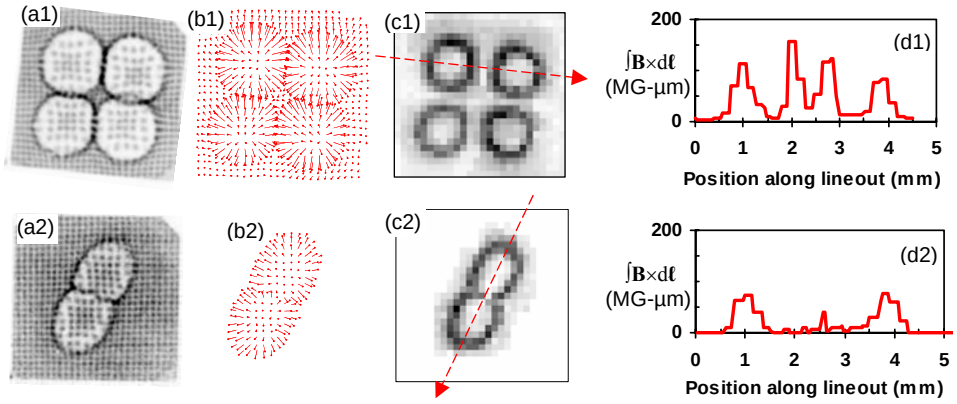

FIG. 4. (Color) Radiography images were used to deduce maps of the B field at the foil. In a1 and a2, from Figs. 2A and 2B, the location of each beamlet can be compared with the location it would have had with no B fields (beamlets on the image edges define the grid of "undeflected" locations); b1 and b2 show displacement vectors ξ. Arrays of displacement amplitudes are shown as images (c1 and c2); each pixel represents one beamlet, with value proportional to displacement. Displacement is proportional to $\int B\times d\ell$ along the particle trajectory, so lineouts of c1 and c2 (along the red arrows) provide quantitative measurements of $|\int \mathbf{B}\times d\boldsymbol{\ell}|$ at the foil location (d1 and d2).

To place these measurements in the broader context of basic plasma physics, we can calculate the Magnetic Reynolds number

$$R_m = \frac{L_\perp \mathrm{v}}{D_m} \approx \frac{\nabla\times(\mathbf{v}\times\mathbf{B})}{\nabla\times(D_m\nabla\times\mathbf{B})} \quad , \qquad (2)$$

where $L_\perp \approx T_e/\nabla T_e \sim 50\text{-}100$ μm is a characteristic length scale. When the laser is on, $R_m >> 1$ (v is the high bubble expansion velocity $v_b \sim 5\times10^7$ cm s^{-1} and diffusion $D_m \sim 4\times10^2$ cm^2 s^{-1} is low), so the fields must be frozen in and move with the plasma. And because of the high value of β (>>1), the plasma flow is not significantly affected by the fields despite their MG levels. The bubble expansion in this regime can be approximately described as "free-streaming" because the velocity is of the order of the ion sound velocity ($C_s \sim 2\times10^7$ cm s^{-1}).

Returning to germane results in the 4-beam data, there is little or no interaction between field structures localized to different bubble surfaces at the earliest times (Figs. 4c1, 4d1). The integrals under the individual peaks shown in Fig. 4d1 are approximately equal [$\sim(5.0\pm0.5)\times10^4$MG-μm^2], indicating little if any field cancellation. At these times, the field lines retain their original topology, ie. closed loops around each beam spot. Eventually, the separate bubbles touch each other; they mix fields with opposing directions, which cancel each other. The sharp gradients in density and temperature at the edges of the individual bubbles (Fig. 3) must diminish as the bubbles coalesce, removing the principal field-generating mechanism ($\nabla n_e \times \nabla T_e$). The result of this field reconnection is exactly what we see in the field map of Fig. 4c2, which shows diminished field strength at the point of bubble intersection, and in the lineout of Fig. 4d2. Integrals under the lineout portions representing the walls of the bubbles are $\sim4\times10^4$ MG-μm^2 for each outer wall and $\sim 4\times10^3$ MG-μm^2 for the two overlapping walls; this indicates at least a 95% reduction in $|\int \mathbf{B}\times d\boldsymbol{\ell}|$ in the intersection region. Based on these measured numbers and the observed scale sizes for the magnetic bubble, the total magnetic energy converted to plasma internal energy in the reconnection region was $\sim2.5\times10^2$ J cm^{-3}. Taking the electron density around the bubble edge to be ~1-10% of the critical density ($n_c \sim 10^{22}$ cm^{-3}), we estimate the resulting rise in plasma temperature to be 1-10 eV, a small and presently immeasurable fraction (≤ 1%) of the T_e (~1 keV). This is expected for our high-β plasma; the reconnection energy has little impact on the dynamics of the interacting bubbles.

To further illuminate the nature of reconnection in this high-β, HED experiment, the data can be compared to predictions of the standard Sweet-Parker (SP) model [20,21] of resistive reconnection (though SP is in fact a steady state model, making this comparison qualitative, at best). The experimental time scale for reconnection can be estimated as $\tau_{R,E} \sim 0.2$ ns by dividing the apparent width of the field layer at the surface of the bubble in Fig. 4c1 by twice the bubble expansion velocity. In contrast, the SP reconnection time is $\tau_{R,SP} = (\tau_D \tau_A)^{1/2} \sim 5$ ns, where $\tau_D = 0.5 L_\perp^2 D_m^{-1} \sim 30$ ns is the B-field diffusion time, $\tau_A = L_\perp v_A^{-1} \sim 1$ ns is the Alfvén transit time, and $v_A \sim 5\times10^6$ cm s^{-1} (taking $n_i \sim 1\times10^{20}$ cm^{-3} and inferring, from Fig. 4 and earlier results [11], that B ~0.5 MG for a proton path length ~200 μm). Though there are uncertainties in the estimates of these parameters, the comparison suggests that the reconnection illustrated in Figs. 4a2-4d2 is dominated by plasma hydrodynamics and noncollisional (nondissipative) processes, rather than resistivity. This dominance is connected with the fact that the plasma expansion velocity is faster than the Alfvén velocity. Unlike all previous reconnection experiments, the ones described here have a reconnection time shorter than the characteristic Alfvén transit time.

The observations described here provide the first precise measurements and mapping of the change in field topology associated with reconnection in a high-β, HED experiment; they involve the merging of either 2 or 4 hemispherical plasma bubbles in which MG fields thread the boundary of each bubble. The unique methodology described herein is applicable to a wide class of basic and applied plasma experiments for which exact and comprehensive field maps are required during the generation, growth, interaction, and dissipation of complex B field structures.

The work described here was performed in part at the LLE National Laser User's Facility (NLUF), and was supported in part by US DOE (Grant No. DE-FG03-03SF22691), LLNL (subcontract Grant No. B504974), and LLE (subcontract Grant No. 412160-001G).

[1] D. Biskamp *Magnetic Reconnection in Plasmas* (Cambridge University press, Cambridge 2000).
[2] S. Masuda *et al., Nature* **371**, 495 (1994).
[3] T. D. Phan *et al., Nature* **439**, 175 (2006).
[4] J. B. Taylor, *Rev. Mod. Phys.* **58**, 741 (1986).
[5] J. Nuckolls *et al.*, *Nature* **239**, 139 (1972).
[6] M. A. Yates *et al.*, *Phys. Rev. Lett.* **49**,1702 (1982).
[7] R. C. Davidson, *Frontiers in High Energy Density Physics* (National Academies Press, Washington,2003).
[8] R. P. Drake, *High-Energy-Density Physics* (Springer Press, New York, 2006).
[9] B. A. Remington *et al.*,*Science* **284**, 1488 (1999).
[10] C. K. Li *et al.*, *Rev. Sci. Instrum.* **77**, 10E725 (2006).
[11] C. K. Li *et al.*, *Phys. Rev. Lett.* **97**, 135003 (2006).
[12] A. Mackinnon *et al.*, *Rev. Sci. Instrum.* **75**, 3531 (2004).
[13] P. Nilson *et al.*, *Phys. Rev. Lett.* **97**, 255001(2006).
[14] S. I. Braginskii, *Review of Plasma Physics* 1 (Consultants Bureau, New York, 1965).
[15] M. G. Haines, *Phys. Rev. Lett.* **78**, 254 (1997).
[16] C. K. Li *et al.*, Submitted to *Phys. Rev. Lett.* (2006).
[17] T. R. Boehly *et al.*, *Opt. Commun.* **133**, 495 (1997).
[18] T. J. Kessler *et al.*, *Laser Coherence Control: Technology and Applications* (SPIE, Bellingham, WA 1993).
[19] F. Séguin *et al.*, *Rev. Sci. Instrum.* **75**, 3520(2004).
[20] P. A. Sweet, *Nuovo Cimento Suppl.* **8**, Ser.X, 188(1958).
[21] E. N. Parker, *Astrophys. J. Suppl. Ser.* **8** 177 (1963).
[22] G. B. Zimmerman *et al., Comm. in Plasm. Phys. and Contr. Fus.* **2**, 51 (1975).